2016.01.20 astro-ph Seminar (担当 大澤)

A New Star-Formation Rate Calibration from Polycyclic Aromatic Hydrocarbon Emission Features and Application to High Redshift Galaxies

H. V. Shipley et al. accepted for publication in ApJ

Abstract & Introduction

We calibrate the integrated luminosity from the polycyclic aromatic hydrocarbon (PAH) features at 6.2μm, 7.7μm and 11.3μm in galaxies as a measure of the star-formation rate (SFR). These features are strong (containing as much as 5-10% of the total infrared luminosity) and suffer minimal extinction. Our calibration uses *Spitzer* Infrared Spectrograph (IRS) measurements of 105 galaxies at $0 < z < 0.4$, infrared (IR) luminosities of $10^9 - 10^{12} L_\odot$, combined with other well-calibrated SFR indicators. The PAH luminosity correlates linearly with the SFR as measured by the extinction-corrected Hα luminosity over the range of luminosities in our calibration sample. The scatter is 0.14 dex comparable to that between SFRs derived from the Paα and extinction-corrected Hα emission lines, implying the PAH features may be as accurate a SFR indicator as hydrogen recombination lines. The PAH SFR relation depends on gas-phase metallicity, for which we supply an empirical correction for galaxies with $0.2 < Z \lesssim 0.7\ Z_\odot$. We present a case study in advance of the *James Webb Space Telescope* (*JWST*), which will be capable of measuring SFRs from PAHs in distant galaxies at the peak of the SFR density in the universe ($z \sim 2$) with SFRs as low as $\sim 10\ M_\odot\ yr^{-1}$. We use *Spitzer*/IRS observations of the PAH features and Paα emission plus Hα measurements in lensed star-forming galaxies at $1 < z < 3$ to demonstrate the ability of the PAHs to derive accurate SFRs. We also demonstrate that because the PAH features dominate the mid-IR fluxes, broad-band mid-IR photometric measurements from *JWST* will trace both the SFR and provide a way to exclude galaxies dominated by an AGN.

Keywords: galaxies: active — galaxies: evolution — galaxies: high-redshift — infrared: galaxies

- z ~ 1–3 でも有効かつ extinction free な SFR の指標が欲しい！→ PAH をつかおう
- これまで Spitzer で観測された天体から解析にふさわしいサンプルを選択
- 金属量が太陽程度の場合 $\log_{10} L_{PAH}$ は他の SFR の指標とよい相関を示した
- 低金属量の銀河の場合は傾向からずれるが金属量で補正可能である
- 分光せずに broad band photometry でもそこそこの精度が出そう
- JWST の MIRI は z ~ 1–3 の SFR 統計を取るのにいい仕事します

3 種類のサンプルを用意

- **calibration sample (227):**
  O' Dowd+ (2009), Shipley+ (2013), Brown+ (2014) から十分な S/N と分光データがあるもの
- **primary calibration sample (105):**
  calibration sample から solar-Z かつ星形成銀河をセレクト ($z \sim 0.0$–0.4, $10^9 L_\odot < L_{IR} < 10^{12} L_\odot$)
- **demonstration sample (7):**
  重力レンズで増光した z ~ 1–3 の銀河 (high-z での検証用)

Figure 1. PAH feature 強度の測定

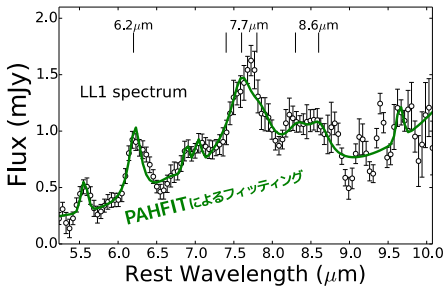

$$SFR\ (M_\odot\ yr^{-1}) = 5.5 \times 10^{-42} [L(H\alpha) + 0.020\, L(24\ \mu m)]\ (erg\ s^{-1})$$

$$L_{PAH} = L_{6.2\mu m} + L_{7.7\mu m} + L_{11.3\mu m}$$

$$\log L_{PAH} = (1.30 \pm 0.03) + \log(L_{H\alpha} + 0.020 \times L_{24\ \mu m})$$

$$\log SFR\ (M_\odot\ yr^{-1}) = (-42.56 \pm 0.03) + \log L_{PAH}\ (erg\ s^{-1})$$

Figure 6. PAH SFR と Hα SFR の比較

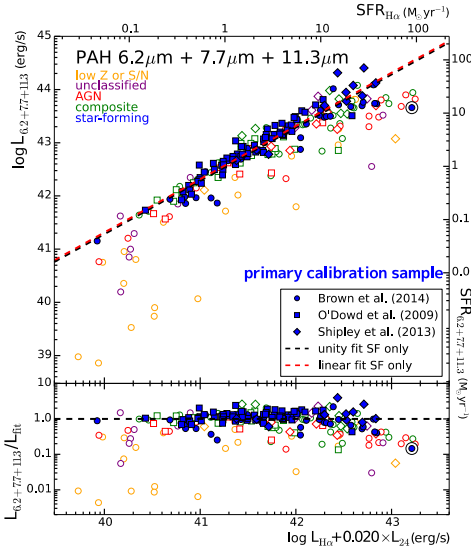

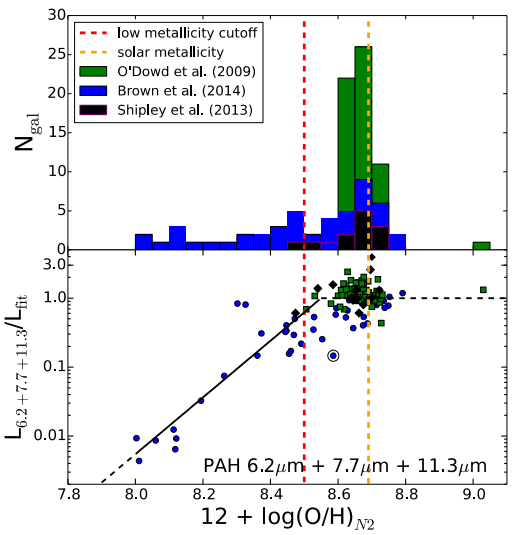

Figure 9. 低金属量環境での補正項

$$\log L_{PAH,\lambda}^{corr} = \log L_{PAH,\lambda} - A[Z - (Z_\odot + Z_0)]$$
for $12 + \log(O/H)_{N2} \leq 8.55$
where $Z_0 = -0.14$

Metallicity Corrections

PAH Feature(s)	A
6.2 + 7.7 + 11.3	4.1 ± 0.3
6.2	4.0 ± 0.3
7.7	4.0 ± 0.3
11.3	3.7 ± 0.3
6.2 + 7.7	4.1 ± 0.4
6.2 + 11.3	3.8 ± 0.3
7.7 + 11.3	4.1 ± 0.3

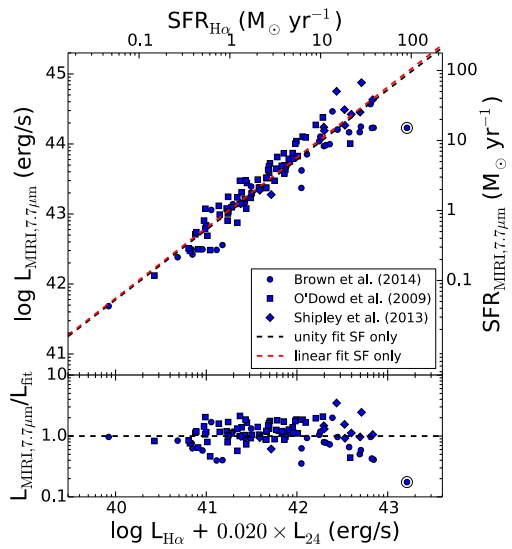

Figure 10. JWST/MIRI 広帯域フィルタでの予想

$$\log SFR\ (M_\odot\ yr^{-1}) = (-43.05 \pm 0.06) + \log L_{7.7\mu m}(erg\ s^{-1})$$

Table 5
Demonstration Sample SFRs

SFR Indicator	A2218b	A2667a	The Clone	A2218a	A1835a	cB58	8 O'clock
	z = 1.034	1.035	2.003	2.520	2.566	2.729	2.731
Paα	…	…	< 6.5	61.2 ± 12.9	557. ± 105.	< 22.0	266. ± 29.4
Hα + 24μm	32.5 ± 1.3	35.5 ± 0.5	25.1 ± 1.5	45.1 ± 3.2	223. ± 21.2	21.1 ± 2.9	139. ± 10.9
6.2 + 7.7 + 11.3	27.2 ± 0.5	10.8 ± 0.3	8.3 ± 0.3	…	…	…	…
6.2	27.5 ± 0.3	8.1 ± 0.1	15.0 ± 0.6	68.6 ± 3.4	211. ± 39.4	11.1 ± 0.8	302. ± 20.0
7.7	28.5 ± 0.7	11.7 ± 0.4	7.3 ± 0.2	53.3 ± 1.3	168. ± 10.3	8.5 ± 0.4	262. ± 36.7
11.3	25.3 ± 1.0	11.4 ± 0.7	7.6 ± 1.2	…	…	…	…
6.2 + 7.7	27.9 ± 0.6	10.8 ± 0.3	8.6 ± 0.2	55.3 ± 1.2	173. ± 11.0	8.8 ± 0.4	265. ± 29.6
6.2 + 11.3	25.1 ± 0.5	9.4 ± 0.4	10.5 ± 0.7	…	…	…	…
7.7 + 11.3	27.7 ± 0.6	11.5 ± 0.4	7.3 ± 0.3	…	…	…	…

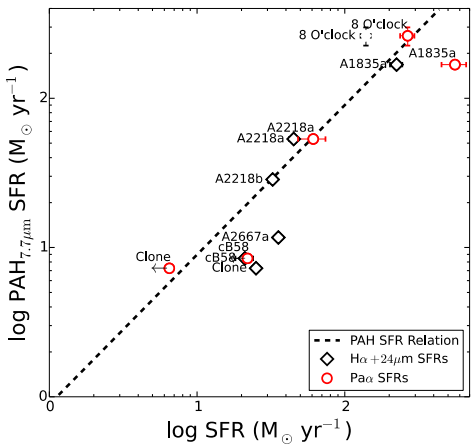

Figure 11. z ~ 1–3 でのデモンストレーション

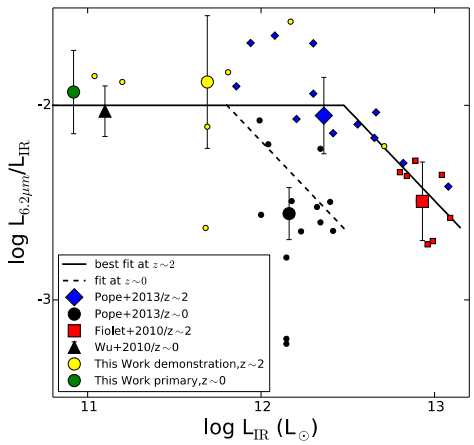

Figure 12. high-z ULIRG での L_{PAH} 減少傾向